

Research Paper

Regulation of ezrin tension by S-nitrosylation mediates non-small cell lung cancer invasion and metastasis

Xiaolong Zhang^{1,2*}, Guangming Li^{3*}, Yichen Guo⁴, Ying Song⁵, Linlin Chen^{1,2}, Qinli Ruan^{1,2}, Yifan Wang^{1,2}, Lixia Sun⁶, Yunfeng Hu^{1,2}, Jingwen Zhou⁷, Bin Ren⁴, Jun Guo^{1,2}✉

1. State Key Laboratory Cultivation Base for TCM Quality and Efficacy, School of Medicine and Life Science, Nanjing University of Chinese Medicine, Nanjing 210023, Jiangsu, PR China.
2. Key Laboratory of Drug Target and Drug for Degenerative Disease, Nanjing University of Chinese Medicine, Nanjing 210023, Jiangsu, PR China.
3. Department of Anesthesiology, Huaian First People's Hospital, Nanjing Medical University, Huaian 223001, Jiangsu, PR China.
4. Department of Surgery and Biomedical Engineering, University of Alabama at Birmingham (UAB), Birmingham, Alabama. 35294, USA.
5. Department of Respiratory Medicine, The First Affiliated Hospital of Nanjing Medical University, Nanjing 210029, PR China
6. Affiliated Hospital of Nanjing University of Chinese Medicine, Nanjing 210023, Jiangsu, PR China.
7. The First Clinical Medical College of Nanjing University of Chinese Medicine, Nanjing, Jiangsu 210023, PR China.

* contributed equally to this work

✉ Corresponding author: Jun Guo, Ph.D., Department of Biochemistry and Molecular Biology, School of Medicine and Life Science, Nanjing University of Chinese Medicine, Nanjing 210023, PR China, Tel/Fax: 86-25-85811707, E-mail: guoj@njucm.edu.cn.

© Ivyspring International Publisher. This is an open access article distributed under the terms of the Creative Commons Attribution (CC BY-NC) license (<https://creativecommons.org/licenses/by-nc/4.0/>). See <http://ivyspring.com/terms> for full terms and conditions.

Received: 2018.12.21; Accepted: 2019.03.18; Published: 2019.04.13

Abstract

Cancer invasion and metastasis depend on accurate and rapid modulation of both chemical and mechanical activities. The S-nitrosylation (SNO) of membrane cytoskeletal cross-linker protein ezrin may regulate the malignant process in a tension-dependent manner.

Methods: The level of nitrosylated ezrin in non-small cell lung cancer (NSCLC) tissues and A549 cell line were evaluated by biotin-switch assay. A few cysteine mutated plasmids of ezrin were used to identify active site for SNO. Newly designed ezrin or mutated-ezrin tension probes based on Förster resonance energy transfer (FRET) theory were applied to visually observe real-time tension changes. Cytoskeleton depolymerizing and motor molecular inhibiting experiments were performed to reveal the alternation of the mechanical property of ezrin after SNO. Transwell assays and xenograft mouse model were used to assess aggressiveness of A549 cells in different groups. Fluorescent staining was also applied to examine cellular location and structures.

Results: High inducible nitric oxide synthase (iNOS) levels were observed to induce ezrin-SNO, and then promote malignant behaviors of NSCLC cells both in vitro and in vivo. Cys¹¹⁷ was identified as the only active site for ezrin-SNO. Meanwhile, an increased level of ezrin tension was observed after iNOS-induced SNO. Enhanced ezrin tension was positively correlated with aggressiveness of NSCLC. Moreover, Microfilament (MF) forces instead of microtubule (MT) forces played dominant roles in modulating ezrin tension, especially after ezrin nitrosylation.

Conclusion: This study revealed a SNO-associated mechanism underlying the mechanical tension of ezrin. Ezrin-SNO promotes NSCLC cells invasion and metastasis through facilitating mechanical transduction from the cytoskeleton to the membrane. These studies implicate the therapeutic potential by targeting ezrin in the inhibition NSCLC invasion and metastasis.

Key words: non-small cell lung cancer; ezrin S-nitrosylation; FRET; invasion; metastasis

Introduction

Non-small cell lung cancer (NSCLC), accounts for approximately 85% of lung cancer, is still a big

challenge worldwide [1]. Despite the improvement in therapeutic strategies, the overall survival of NSCLC

patients yet remains at a low level which is predominantly attributed to tumor metastasis [2]. Therefore, identifying novel mechanisms that underlie the invasion and metastasis of NSCLC are clearly warranted.

Protein S-nitrosylation (SNO) is a nitric oxide-dependent post-translational modification of cysteine, which is an important regulator of cellular functions [3]. In eukaryotic cells, NOS family proteins, especially inducible NOS (iNOS; NOS2) [4], are the major endogenous nitric oxide (NO) donors, which contribute to cellular S-nitrosylation. In the lung microenvironment, endogenous or exogenous insults such as silica, smoking, and bronchitis, which result in a chronic inflammatory state, are major risk factors for carcinogenesis [5]. Numerous pro-inflammatory and anti-inflammatory cytokines (e.g., tumor necrosis factor alpha (TNF- α), interleukin (IL)-1 β , IL-6 and interferon- γ (IFN- γ) [6, 7]) caused by the complex pulmonary microenvironment can induce excessive iNOS and high efflux of NO in alveolar macrophages and pulmonary epithelial cells. This pathologically high levels of iNOS/NO can promote protein-SNO, which is involved in multiple biological processes of cancer [8], for example, NO stress plays a role in promoting tumor growth through DNA damage and genome instability [9]. However, the relationship between protein-SNO and lung cancer aggressive properties remains unclear.

Ezrin is a member of ezrin-radixin-moesin (ERM) family, a class of membrane-cytoskeleton linker proteins. ERM proteins locate in cellular structures where the plasma membrane proteins interact with the actin cytoskeleton and maintain the structural stability and cortical integrity of cells [10]. In NSCLC, ezrin expression is higher in the primary cancer tissues than in matched normal lung tissues [11], and the abnormal expression of ezrin is associated with higher metastatic potential and lower patient survival [12]. Possessing two cysteine residues, ezrin is thought to be capable for nitrosylation modification. However, the physiological or pathological role of ezrin-SNO remains to be elucidated.

Mechanical forces are involved in ubiquitous biological processes [13], but the underlying mechanical mechanism in cancer motility remains incompletely understood. As a linker protein, ezrin functions to transduce mechanical signal from the membrane to the cytoskeleton and is involved in multiple cellular processes especially in cancer invasion and metastasis [12, 14]. However, whether ezrin-SNO regulates ezrin's mechanical properties and NSCLC aggressiveness remains to be clarified.

In the present study, we investigated the mechanisms underlying iNOS mediated ezrin-SNO and its relationship with NSCLC aggressiveness. In addition, using a newly designed ezrin tension probe based on the Förster resonance energy transfer (FRET) theory, we observed real-time ezrin tension changes during tumor progression visually and reveal the role of ezrin-SNO in modulating the mechanical property of ezrin during NSCLC cells invasion and metastasis.

Methods

Cell Culture

The A549 cell line was acquired from the American Type Culture Collective (ATCC) (Manassas, Virginia, USA) and authenticated by Genetic Testing Biotechnology Corporation (Suzhou, China) using short tandem repeat (STR) profiling. Mycoplasma contamination was tested using the Mycoplasma Plus PCR Primer Set (Agilent, Santa Clara, USA) and were found to be negative. Cells were cultured in Dulbecco's Modified Eagle's Medium (Gibco, New York, USA) containing 10% fetal bovine serum (Gibco, New York, USA) and a mixture of 100 units/mL penicillin and 100 μ g/mL streptomycin (Gibco) at 37 °C and 5% CO₂.

Antibodies and Reagents

Commercially available antibodies included: ezrin (Cell Signaling Technology, Danvers, USA); β -actin (Boster, Wuhan, China); α -tubulin (Boster); NOS2 (Immunoway, Wuhan, China). Secondary anti-rabbit and anti-mouse antibodies (Cell Signaling Technology), human IL-6 (Bioss, Beijing, China); human IFN- γ (NOVUS, Colorado, USA); 1400W (Beyotime, Shanghai, China); L-N^G-monomethyl arginine citrate (L-NMMA) (Beyotime); C-X-C motif chemokine 12 (CXCL12) (Peprotech, Rocky Hill, USA); (-)-blebbistatin (MCE, New Jersey, USA); ispinesib (Selleck, Houston, USA); nocodazole (MCE); cytochalasin B (Aladdin, Shanghai, China); E.Z.N.A Endo-free Plasmid DNA Mini Kit II (OMEGA, Doraville, USA); S-nitrosylated Protein Detection Kit (Cayman, Michigan, USA); X-tremeGENE HP DNA transfection reagent (Roche, Basel, Switzerland); geneticin (Sigma, Darmstadt, Germany); Protein A/G PLUS-agarose bead (Santa Cruz Biotechnology, CA, USA); and basement membrane matrix (Corning, New York, USA).

Immunoprecipitation

Cells were grown in complete medium overnight, treated with IL-6 (10 ng/mL), IFN- γ (50 ng/mL) and a cytokine mixture (IL-6, 10 ng/mL; IFN- γ , 50 ng/mL) for 12 h. Cell lysates were incubated with anti-ezrin antibodies and immunoprecipitated

with Protein A/G -agarose beads overnight. Immunoprecipitates were denatured by boiling in loading buffer and then cooled down before western-blotting analysis.

Western blotting

Cell lysates were denatured by boiling in loading buffer. SDS-PAGE was performed, and proteins were transferred to nitrocellulose membranes (Bio-Rad, California, USA). After blocking in 5% non-fat milk for 1 h, the membranes were incubated with mouse- or rabbit-derived primary antibodies overnight and then with homologous secondary antibodies. Immunoreactive bands were visualized using enhanced chemiluminescence (Bio-Rad). Densitometric analysis was performed for normalization.

Immunofluorescence

Cells were grown on a glass bottomed cell culture dish. After adequate fixture and permeabilization, all the samples were blocked in 4% bovine serum albumin. Subsequently, the samples were incubated with mouse- or rabbit-derived primary antibodies, followed by fluorescein isothiocyanate (FITC)-conjugated or tetramethylrhodamine (TRITC)-conjugated homologous secondary antibodies. 4, 6-diamidino-2-phenylindole (DAPI) was used for DNA staining. To detect microfilament morphology, samples were additionally incubated with FITC-conjugated phalloidin. The samples were imaged under an inverted fluorescence microscope.

Detection of protein-SNO by immunoprecipitation

Protein-SNO was detected using S-nitrosylated Protein Detection Kit (Cayman) with slight modifications. Briefly, according to the manufacturer's procedure, cells were lysed in lysis buffer containing the thiol-specific methylthiolating reagent (methyl methanethiosulfonate, MMTS) to block free reactive thiol groups. The supernatants were transferred to a new polypropylene tube after centrifugation and subjected to acetone precipitation to remove free MMTS. Buffers containing reducing and labeling reagents (biotin-HPDP and ascorbic acid sodium salt) were used to resuspend the pellets in order to switch the SNO site into biotin-tag. Acetone precipitation was performed again to remove free biotin-HPDP, and the pellets were stored for immunoprecipitation-based ezrin-SNO analysis. Next, NP-40 lysis buffer was used to dissolve the protein pellets, followed by anti-ezrin immunoprecipitation to analyze ezrin-SNO levels. A preliminary experiment was performed to normalize the total ezrin level. Subsequently, total ezrin (by HPR-conjugated secondary antibody) and ezrin-SNO

(by HPR-conjugated Avidin) were detected respectively. Control experiments were performed by omission of the reducing and labeling reagents.

Clinical samples and Kaplan–Meier survival analysis

Fresh lung cancer tissue samples and adjacent normal tissues were obtained by surgery from the Thoracic Surgery Department of Affiliated Hospital of Nanjing University of Chinese Medicine (Nanjing, China). Informed consent was obtained from all patients and ethical approvals for this study were obtained from the Institutional Review Board of Human Research of the Affiliated Hospital of Nanjing University of Chinese Medicine. The clinical features of the patients are listed in Table S1. For the survival analyses, data were obtained from the Kaplan-Meier plotter database, and all the patients were sorted into different groups and tested for significance using log-rank tests.

Cell invasion and migration assays

The transwell apparatus (Corning, New York, USA) was pre-coated with 50 μ L of matrigel solution in upper chamber. A549 cells (2×10^5) were starved overnight and seeded into the upper chamber in serum-free medium, and medium supplemented with 20% FBS was added to the bottom chamber. After 24 h of incubation, the cells invading into the lower membrane surface were fixed and stained with 0.4% crystal violet. Typical images of invading cells were obtained for statistical analysis. The migration assay was similar to the invasion assay, except for pre-coating with matrigel.

Small interfering RNA (siRNA) design and plasmid construction

The siRNA targeting ezrin was constructed by Sangon Biotech Co., Ltd (Shanghai, China). The oligonucleotides were:

Sense: 5'-GUGAAGGAAGGAAUCCUATT-3'.

Antisense: 5'-UAAGGAUCCUCCUCCUCCACTT-3'.

The pEGFP-N1 ezrin plasmid was purchased from Addgene (#20680). Based on the plasmid obtained, the newly constructed ezrin mutation and FRET-based sensor were structured according to previous reports [15]. Ezrin Cys¹¹⁷ and Cys²⁴⁸ were mutated into serine for nitrosylation experiments. According to previous principles [16], we constructed an angular-dependent FRET tension sensor with circularly permuted cpVenus and cpCerulean (cpstFRET), which was inserted between Pro⁴⁷⁰ and Pro⁴⁷¹ of ezrin. Plasmids were extracted from single colonies and purified according to the manufacturer's instructions.

Stable cell line development and xenograft studies

A549 cells expressing GFP-tagged wild type ezrin, ezrin-C117S or ezrin-C248S were cultured in medium containing 1000 mg/mL geneticin to screen transfected cells for 7 days. The remaining cells were then subcultured in 500 mg/mL of geneticin for 15 days and then checked cell fluorescence. If 80-90% of the cells were fluorescent, we used these lines for xenograft studies.

Twenty-four female BALB/c nude mice (16-18 g, six-weeks old) were obtained from the Institute of Comparative Medicine of Yangzhou University (Yangzhou, China) and maintained under specific pathogen-free conditions at Nanjing University of Chinese medicine. The mice were randomly assigned to three groups (ezrin-WT ezrin-C117S, and ezrin-C248S).

For each group, 1×10^6 screened cells were resuspended in 50 μ L of medium containing 10 μ L of matrigel and injected into the pleural cavity. Lung nodules and cancer progression were monitored and quantified using ChemStudio PLUS (Jena, Jena, Germany) at different time points. Mice were sacrificed at day 28, and systemic organs were immediately resected for ex vivo evidence of metastatic signals. The lungs and livers of these mice were sent for H&E staining, the lung and liver nodules in serial sections were quantified microscopically.

FRET analysis

We constructed stable single cloning cell lines expressing ezrin, ezrin-C117S, or ezrin-C248S FRET probes, as previous reported [16]. Thereafter, FRET image acquisition was performed on inverted fluorescence microscope equipped with a $\times 63$ oil-immersion objective. The emission spectra were sorted using dual-view-2 (DV-2, MAG Biosystems) so that the cyan and yellow emission wavelengths were detected at the same time (The excitation wavelength (EX) = 436 nm and the emission wavelength (EM) = 535/30 nm for CFP detection and 470/30 nm for YFP detection). The dipole angle between the donor/CFP and the acceptor/YFP determined the effectiveness of FRET. CFP/FRET ratios (the intensity of CFP channel divide the intensity of FRET channel) are positively correlated with FRET efficiency but negatively correlated with force [15, 16].

Statistical analysis

Data analysis was performed using the statistical program SPSS statistics version 20 (IBM Corp., Armonk, NY, USA). Results are presented as the mean \pm SD unless otherwise indicated. Statistical

analyses were performed using two-tailed Student's t-test and one-way analysis of variance (ANOVA) was used for single-factor sample comparisons between multiple groups.

Results

Ezrin and iNOS expression is associated with prognosis of patients with NSCLC with elevated ezrin-SNO levels in NSCLC tissues.

To investigate the association between levels of ezrin and iNOS co-expression and the prognosis of patients with NSCLC, we searched the Kaplan-Meier plotter database [17] for clinical data. 524 patients with lung squamous carcinoma and 720 patients with lung adenocarcinoma patients were sorted into EZR(L)NOS2(L), EZR(L)NOS2(H), EZR(H)NOS2(L) and EZR(H)NOS2(H) (L, low expression; H, high expression) groups. Kaplan-Meier survival analysis showed that there was no significant difference in overall survival among the four groups of patients with lung squamous carcinoma (Figure 1A-B). However, lung adenocarcinoma patients with either high ezrin or high iNOS expression had shorter overall survival than those with low expression of both ezrin and iNOS (Figure 1A-B). We then analyzed the ezrin-SNO level of 20 patients with NSCLC (Table S1) by biotin-switch assay according to the manufacturer's procures (Cayman). The results showed that ezrin-SNO level was elevated significantly in NSCLC samples compared with the paired normal lung tissues (Figure 1C-D, Figure S1A). This finding suggested a positive correlation of ezrin-SNO with NSCLC.

High iNOS levels are required for ezrin-SNO-related metastasis and invasion in the inflammatory microenvironment of NSCLC.

Among the cytokines in inflammatory microenvironment of human NSCLC, abundant IL-6 [18] and IFN- γ [6] are two major inducers of iNOS in lung cancer microenvironment. Next, a cytokine mixture (CM), consisting of IL-6 and IFN- γ , was applied as a cellular iNOS inducer to stimulate a high iNOS inflammatory conditions for protein S-nitrosylation. The transwell assay showed that A549 cells stimulated with IL-6 or IFN- γ or the CM promoted cell invasion and migration compared with blank control (Figure 2A-B). Meanwhile, iNOS-specific inhibitor 1400W significantly inhibited this effect (Figure 2A-B). Co-immunoprecipitation and western blotting assay showed a synergistic effect of IL-6 and IFN- γ in activation of iNOS and its interaction with ezrin (Figure S1C-E). Ezrin

S-nitrosylation detection illustrated that both IL-6 and IFN- γ increased ezrin-SNO levels compared with blank control and the CM increased ezrin-SNO levels in a time-dependent manner. Furthermore, 1400W and nonselective NOS inhibitor L-NMMA reduced the basal ezrin-SNO level in A549, and 1400W significantly inhibited the up-regulation of the ezrin-SNO by CM stimulation (Figure 2C-H, Figure S1B). Notably, since co-treatment of both IL-6 and IFN- γ induced levels of iNOS and consequently an up-regulation of ezrin-SNO, cells in the CM group were more aggressive than those treated with IL-6 or IFN- γ alone. Meanwhile, when the basal ezrin-SNO was down-regulated by the iNOS inhibitor, the aggressiveness of A549 cells was also restrained. These results indicated that cytokines could induce iNOS activation and then increase ezrin-SNO levels, which correlated closely with the malignant behavior of NSCLC.

Cys¹¹⁷ is the key site of ezrin S-nitrosylation contributing to aggressive phenotype of NSCLC in inflammatory milieu.

Ezrin has two cysteine residues (Cys¹¹⁷ and Cys²⁴⁸); therefore, 3 ezrin mutated plasmids (ezrin-C117S, ezrin-C248S and ezrin-both) were constructed to investigate SNO sites of ezrin. The results of the biotin-switch assay indicated that ezrin-C117S and ezrin-both A549 cells dramatically down-regulated the ezrin-SNO levels in the presence or absence of CM stimulation, while ezrin-C248S cells maintained the same level of ezrin-SNO as the wild-type group (Figure 3A-B). In addition, transwell assay revealed that ezrin-C117S and ezrin-both A549 cells displayed attenuated aggressiveness, while ezrin-C248S cells were very aggressive, which were similar to wild-type cells (Figure 3C-D), suggesting that the nitrosylation of ezrin on Cys¹¹⁷ were correlated with A549 invasion and migration. Fluorescent staining showed that, A549 cells with

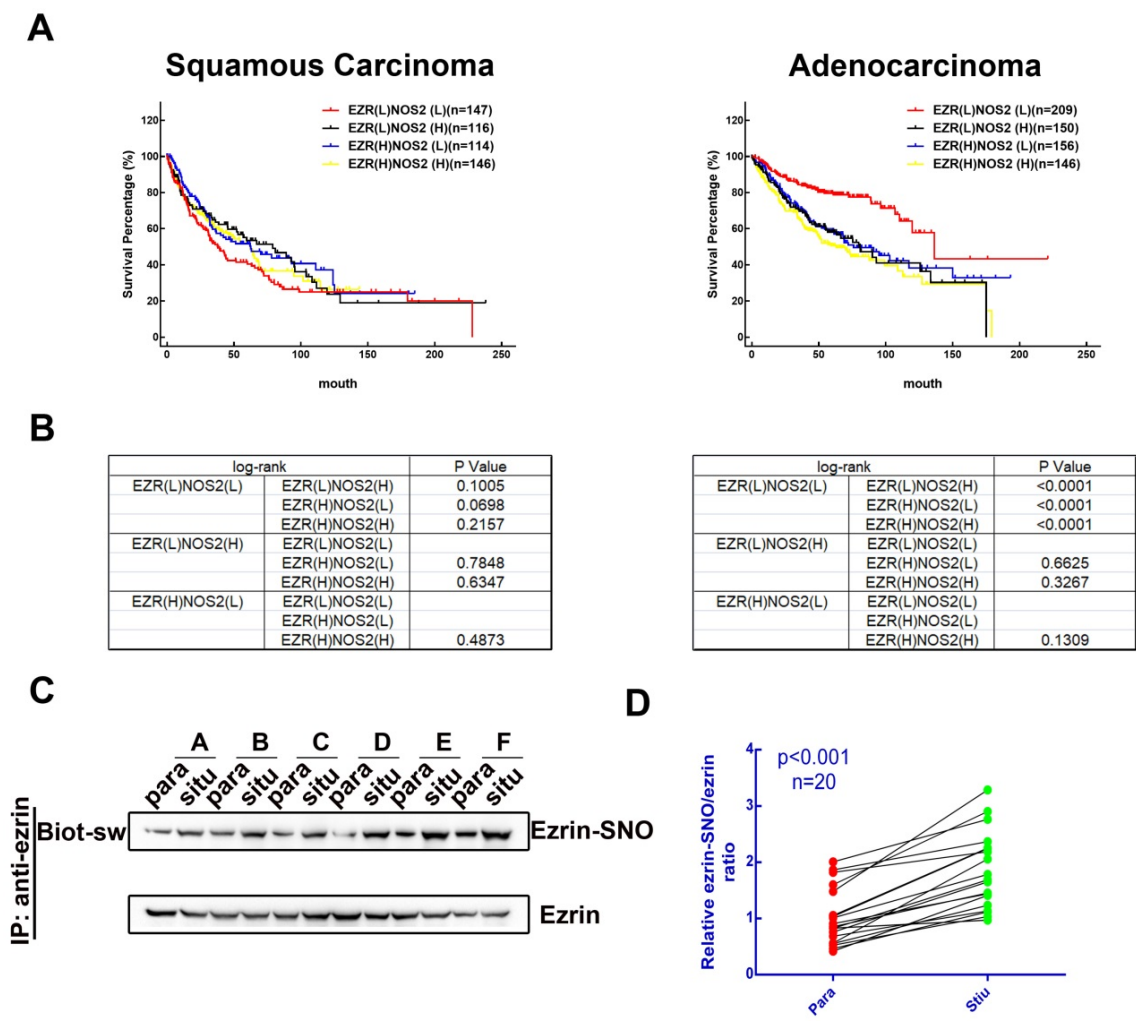


Figure 1. Clinical outcome of patients expressing ezrin and iNOS, and NSCLC have high levels of ezrin-SNO. (A) Kaplan-Meier plots of overall survival of patients with squamous carcinoma and adenocarcinoma. **(B)** Log-rank test between each two groups in squamous carcinoma and adenocarcinoma cases (p value were listed in the table). **(C)** Biotin-switch analysis of ezrin-SNO level in fresh NSCLC tissue (situ) and adjacent normal tissue (para). **(D)** Quantitative analysis from the above of ezrin-SNO/ezrin ratio in NSCLC tissues and matched normal tissues (n = 20).

ezrin-C117S inhibited the function of ezrin for membrane recruitment [19]. However, mutation of Cys²⁴⁸ did not change ezrin binding to the cell membrane (Figure 3E, white arrows). For the MF and MT structure, overexpressing ezrin induced significant cytoskeletal reorganization in wild-type A549 cells as expected [19], especially more filopodia and lamellipodia structures (Figure 3F, white arrows). In A549 cells expressing ezrin-C117S, the numbers of pseudopodium were decreased markedly. Interestingly, a pseudopodium-rich phenotype was

observed in A549 cells expressing ezrin-C248S. Besides, mutation of both cysteine sites resulted in mature pseudopodia structures and an obvious reorganization of MFs. Notably, the MT structures showed no apparent alternation between each group after the CM stimulation (Figure 3F). In summary, ezrin's binding to cell membrane depends on Cys¹¹⁷ nitrosylation mediated by iNOS, which results in MF reorganization, ultimately promoting the aggressive phenotype of NSCLC cells.

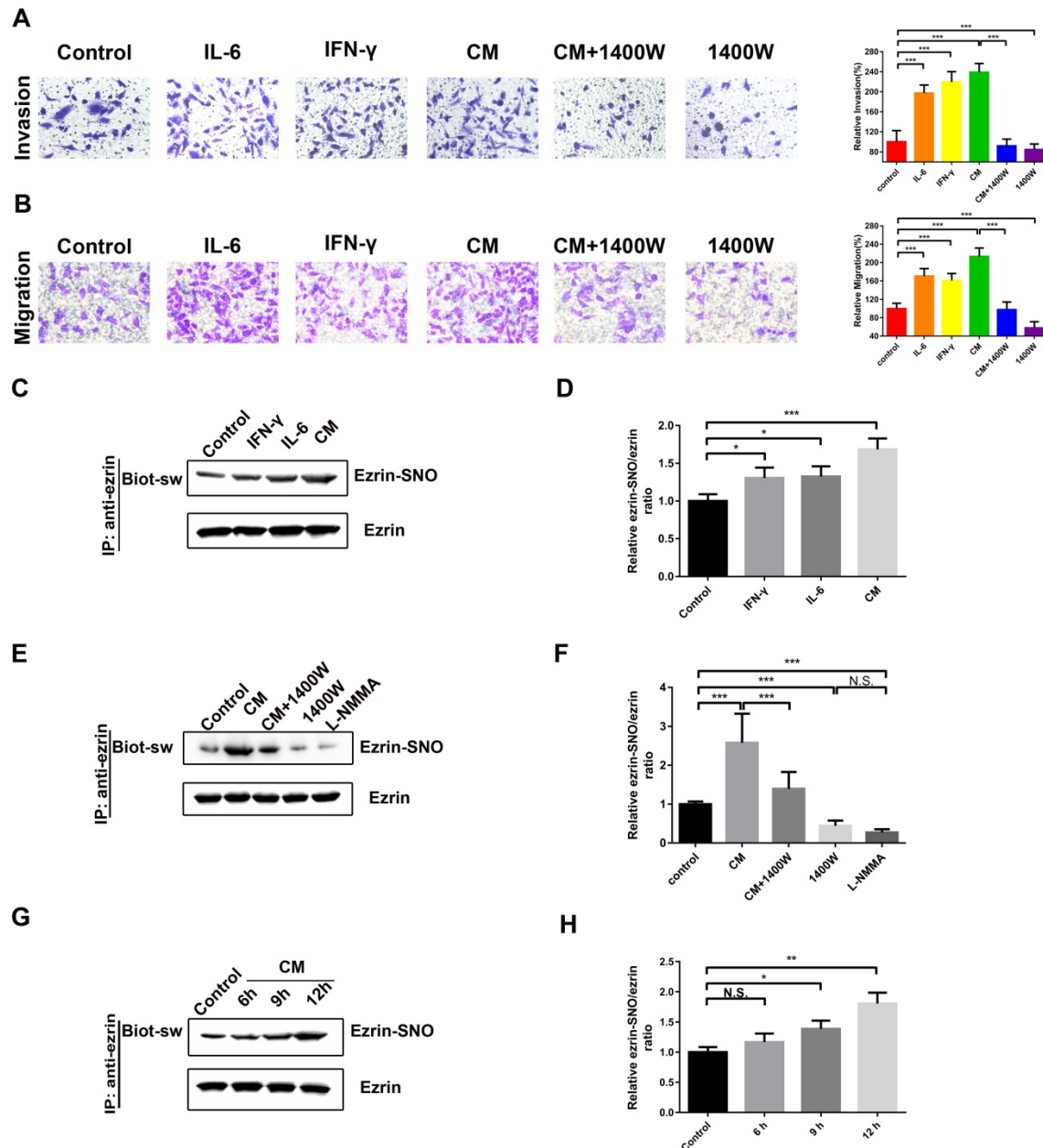


Figure 2. Ezrin-SNO level correlates with malignant behaviors of A549 cells. (A) Representative images of the invasion of A549 cells treated with IL-6, IFN-γ, the CM, the CM+1400W, and 1400W (left panel). (B) Representative images of the migration of A549 cells grouped and treated with reagents as in (A) (left panel). Cell invasion and migration are expressed as a percentage of blank control (right panel) (mean ± SD, n = 3 experiments). (C) Levels of ezrin-SNO in cells treated with IL-6, IFN-γ, and the CM. (E) Levels of ezrin-SNO in cells treated with the CM, the CM+1400W, 1400W, and L-NMMA. (G) Levels of ezrin-SNO in cells treated with the CM in a time-dependent manner. (D), (F), and (H) Relative ezrin-SNO/ezrin ratio was normalized to control value (mean ± SD, n = 3 experiments). One-way ANOVA was used for single-factor sample comparisons. *P < 0.05, **P < 0.01 and ***P < 0.001 for comparison between each group.

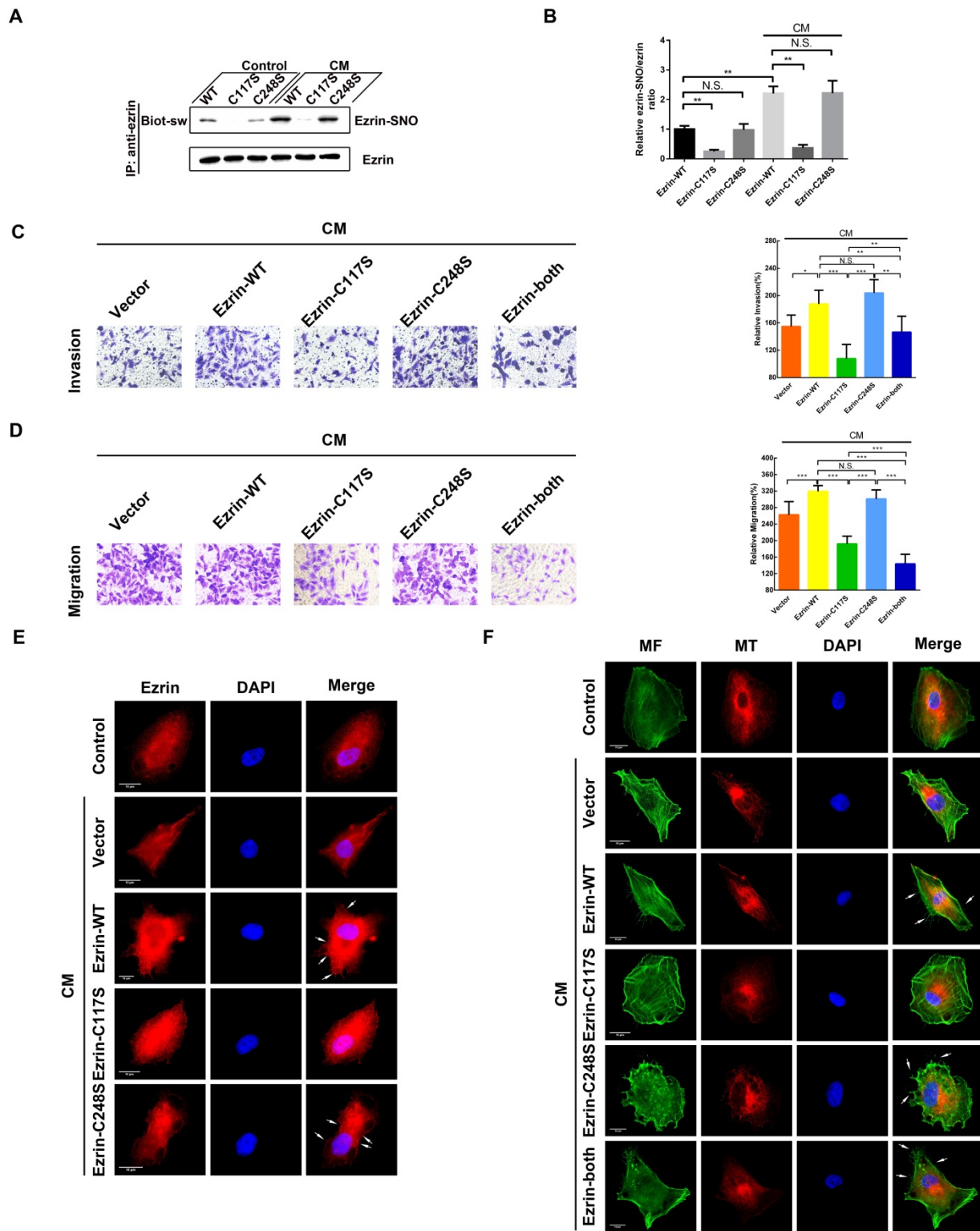


Figure 3. Cys¹¹⁷ is the only active site for ezrin-SNO and correlates with malignant behavior. (A) Levels of ezrin-SNO in cells harboring ezrin-WT, ezrin-C117S, and ezrin-C248S in the presence or absence of cytokine mixture. (B) The relative ezrin-SNO/ezrin ratio was normalized to control value (mean ± SD, n = 3 experiments). (C) Representative images of the invasion of the wild-type ezrin and ezrin mutation cell lines treated with the CM (left panel). (D) Representative images of the migration of A549 cell lines grouping and treating as in (C) (left panel). Cell invasion and migration are expressed as a percentage of control (right panel) (mean ± SD, n = 3 experiments). (E) Representative images of ezrin distribution in cells harboring ezrin-WT, ezrin-C117S, and ezrin-C248S after the CM treatment (TRITC-stained ezrin, red; nucleus, blue; white arrows: the recruitment of ezrin to the cell membrane). (F) Representative images of MT and MF structures in cells harboring ezrin-WT, ezrin-C117S, ezrin-C248S, and ezrin-both after the CM treatment (FITC-stained MFs, green; TRITC-stained MTs, red; nucleus, blue; white arrows: filopodia and lamellipodia structures). Scale bar: 10 μm. One-way ANOVA was used for single-factor sample comparisons. *P < 0.05, **P < 0.01 and ***P < 0.001 for comparison between each group.

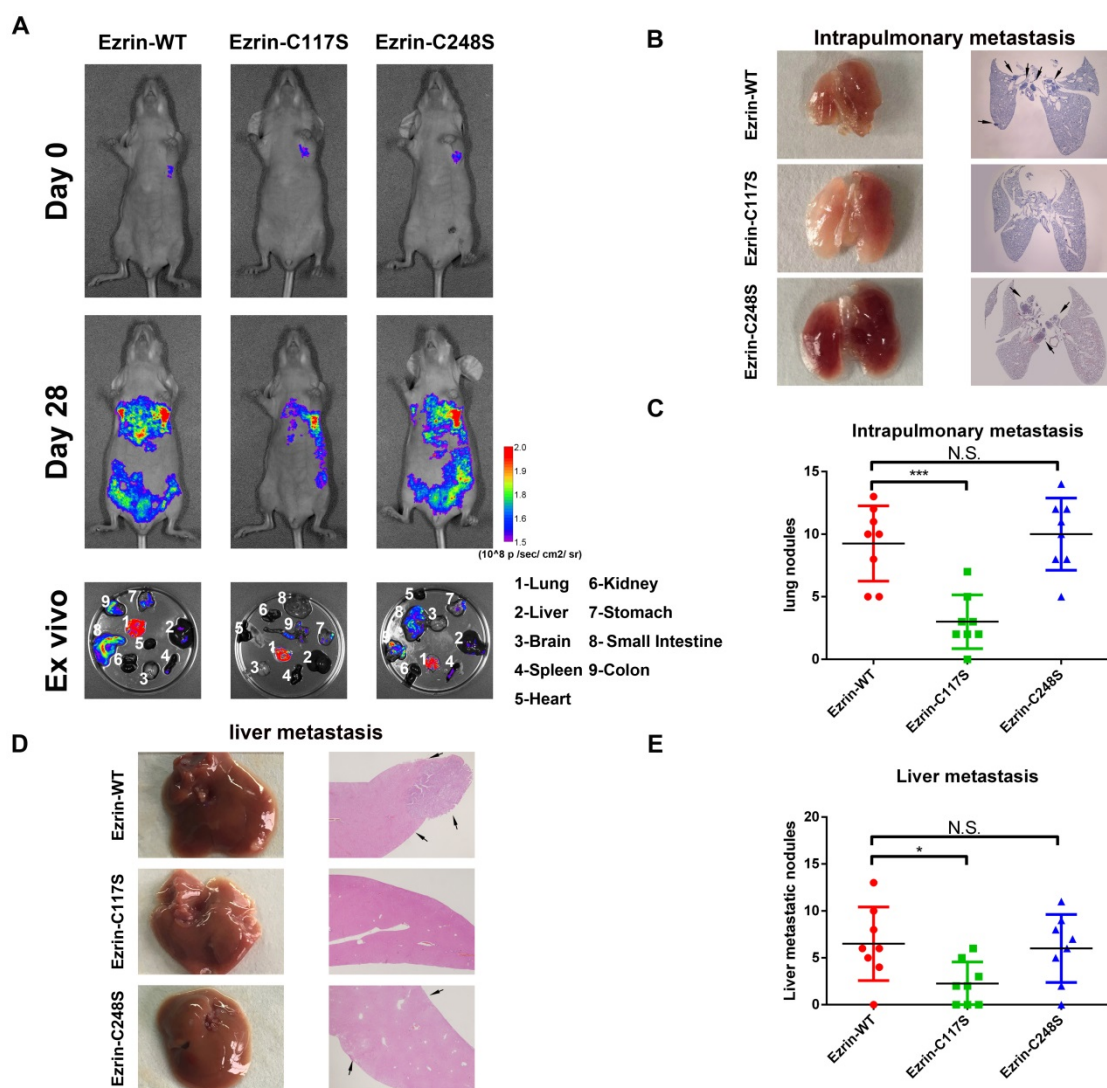


Figure 4. Ezrin Cys¹¹⁷ correlates positively with NSCLC invasion and metastasis in vivo. (A) For the orthotopic implantation assay, bioluminescent images of systemic metastases in nude mice with ezrin-WT, ezrin-C117S, and ezrin-C248S A549 cells are shown. The ex vivo organ metastases including those in the lungs, liver, brain, spleen, heart, kidney, stomach, small intestine, and colon were also presented. (B) Representative images of H&E-stained histological sections of lungs from nude mice in the orthotopic implantation assay (black arrows: metastatic nodules). (C) Box plot showing the numbers of lung nodules from the corresponding mice (mean ± SD, n = 8). (D) Representative images of H&E-stained histological sections of livers from nude mice in the orthotopic implantation assay (black arrows: metastatic nodules). (E) Box plot showing the numbers of liver metastatic nodules from the corresponding mice (mean ± SD, n = 8). Pseudocolor heat-maps indicate the intensity of bioluminescence from low (purple) to high (red) (mean ± SD, n = 8). One-way ANOVA was used for single-factor sample comparisons. ***P < 0.001 compared with ezrin-WT.

Ezrin Cys¹¹⁷ mutation suppresses NSCLC cells invasion and metastasis in vivo.

To further investigate the effect of Cys¹¹⁷-dependent ezrin-SNO on NSCLC cell aggressiveness *in vivo*, we constructed GFP-tagged ezrin-WT, ezrin-C117S, and ezrin-C248S mutated A549 cells.

These cells were then injected into the pleural cavity respectively for the orthotopic implantation assay. The mice receiving ezrin-C117S A549 cells exhibited less spontaneous metastatic signal and distal organ colonization in contrast to ezrin-WT and ezrin-C248S groups (Figure 4A). Meanwhile, Liver and lung histology showed that the number of both intrapulmonary and distant metastatic sites in

ezrin-WT and ezrin-C248S groups were significantly higher than ezrin-C117S group (Figure 4B-C, D-E black arrows), indicating that ezrin-SNO on Cys¹¹⁷ is necessary to promote invasion and metastasis of NSCLC cells.

The construction and test of the ezrin tension sensor.

To test the role of ezrin tension in cell mechanics, we designed a FRET-based tension probe to detect tension in ezrin based on our previous reports [16, 20]. A FRET module was incorporated within the ezrin backbone which reports the real-time resonant energy transfer during angle twisting of the donor-acceptor pair induced by tension loading onto ezrin (Figure S2A-B). In an acceptor bleaching FRET test

(FRET-AB), the transient FRET efficiency of the probe is 21.885% (Figure S2C). In the fluorescence recovery after photobleaching (FRAP) test, the recovery rates for the ezrin in region of interest (ROI) was 39.10% at 500 s after bleaching (Figure S2D). Based on our previous experience, cells generate decreasing or increasing MT/MF forces under hypertonic or hypotonic saline, respectively [21]. We challenged the ezrin-M-cpstFRET transfected cells with hypotonic or hypertonic bathes. The CFP/FRET ratio was used to reveal the tension in ezrin. The results showed an increasing trend of ezrin tension under hypotonic condition and decreasing trend under hypertonic condition which indicated a sensitive alternation of ezrin tension (Figure. S2I-J). However, the FRET efficiency of its control probe, ezrin-C-cpstFRET, remained almost constant (Figure S3A-B). A-cpstFRET-A and T-cpstFRET-T probes were used for the detection of MF and MT force, respectively. Both of them have been strictly tested in our previous works [16, 21].

Ezrin-SNO mediates ezrin tension changes in inflammatory microenvironment of NSCLC cells.

In order to identify the alteration of ezrin's mechanical properties after S-nitrosylation, a stable A549 cell line expressing ezrin-M-cpstFRET tension sensor was challenged with various cytokine stimuli. Intriguingly, compared with blank control, IL-6, IFN- γ , the CM and 1400W did not affect ezrin tension in the first 15 min (Figure 5A-B). However, after 12 h of intervention with IL-6, IFN- γ or the CM, ezrin tension increased compared with that of the blank control group. Co-treatment with the CM and 1400W significantly inhibited ezrin tension and 1400W treatment even decreased ezrin tension below the levels of blank control group (Figure 5C-D). These results revealed that ezrin tension is up-regulated after nitrosylation induced by the high iNOS levels and this may correlate with the high aggressiveness of NSCLC cells.

Cys¹¹⁷ mutation of ezrin suppresses ezrin tension in response to iNOS activation.

To further study the impact of ezrin S-nitrosylation on the mechanical property of the membrane-ezrin-actin apparatus, we mutated relevant cysteine sites (Cys¹¹⁷ and Cys²⁴⁸) of ezrin in the ezrin-M-cpstFRET probe and tested these new probes (Figure S2E-H). Interestingly, in the ezrin-C117S probe transfected A549 cells, the mean CFP/FRET ratio was dramatically decreased in comparison with cells harboring ezrin-WT probe; however, Cys²⁴⁸ mutation had no effect on ezrin tension (Figure 5E-F), an additional experiment of

treating each sable cell line with 1400W for 12 h was performed to determine the role of ezrin-C117S in suppressing ezrin tension. The results showed that 1400W treatment decreased ezrin tension of all three cell lines, suggesting a positive role of basal ezrin-SNO in contributing to the different levels of ezrin tension in different cell lines under control condition (Figure 5E-F). We then treated each group with the CM for 12 h. Cells harboring ezrin-WT or ezrin-C248S tension probe showed a higher tension level, while cells harboring the ezrin-C117S tension probe displayed significantly lower tension (Figure 5G-H), a parallel test for comparing ezrin tension before and after the CM treatment showed approximately no significant alternation of ezrin tension level in ezrin-C117S cell line (Figure S3C-D), suggesting that mutation on Cys¹¹⁷ may hamper nitrosylation related tension growth induced by the CM treatment.

To summarize, the Cys¹¹⁷ mutation of ezrin decreased basal ezrin tension in A549 cells, and inhibited the increase in ezrin tension after CM stimulation, suggesting the attenuated function of ezrin as a mechanical transducer.

Higher ezrin tension correlates with NSCLC cells aggressiveness.

Ezrin contributes to the formation of protrusive structures such as filopodia, lamellipodia, invadopodia [22] which are responsible for cancer invasion and migration [23]. Meanwhile, these dynamic actin-rich membrane structures also function as mechanosensors to regulate these self-organized structures [24]. We performed fluorescent staining to determine the function of ezrin involved in cytoskeleton organization. The overexpression of ezrin increased the formation of filopodia and lamellipodia compared with that in control A549 cells. However, these structures almost disappeared after ezrin knockdown in A549 cells (Figure S4A). Conversely, ezrin had little impact on the microtubule structure (Figure S4B). These morphological changes suggest an important role of ezrin in reorganizing the microfilament cytoskeleton, possibly alternating malignant behavior.

To better understand the mechanical properties of ezrin during NSCLC cells invasion and metastasis, CXCL12 was used to build an aggressive cell model [25, 26] which can serve as an ideal tool to study short-term mechanics in cell. We performed time-lapse imaging for 30 min after adding CXCL12 to isotonic saline in A549 cells. The FRET analysis showed that ezrin tension increased gradually, accompanied by increases of MT and MF forces (Figure 6A-D).

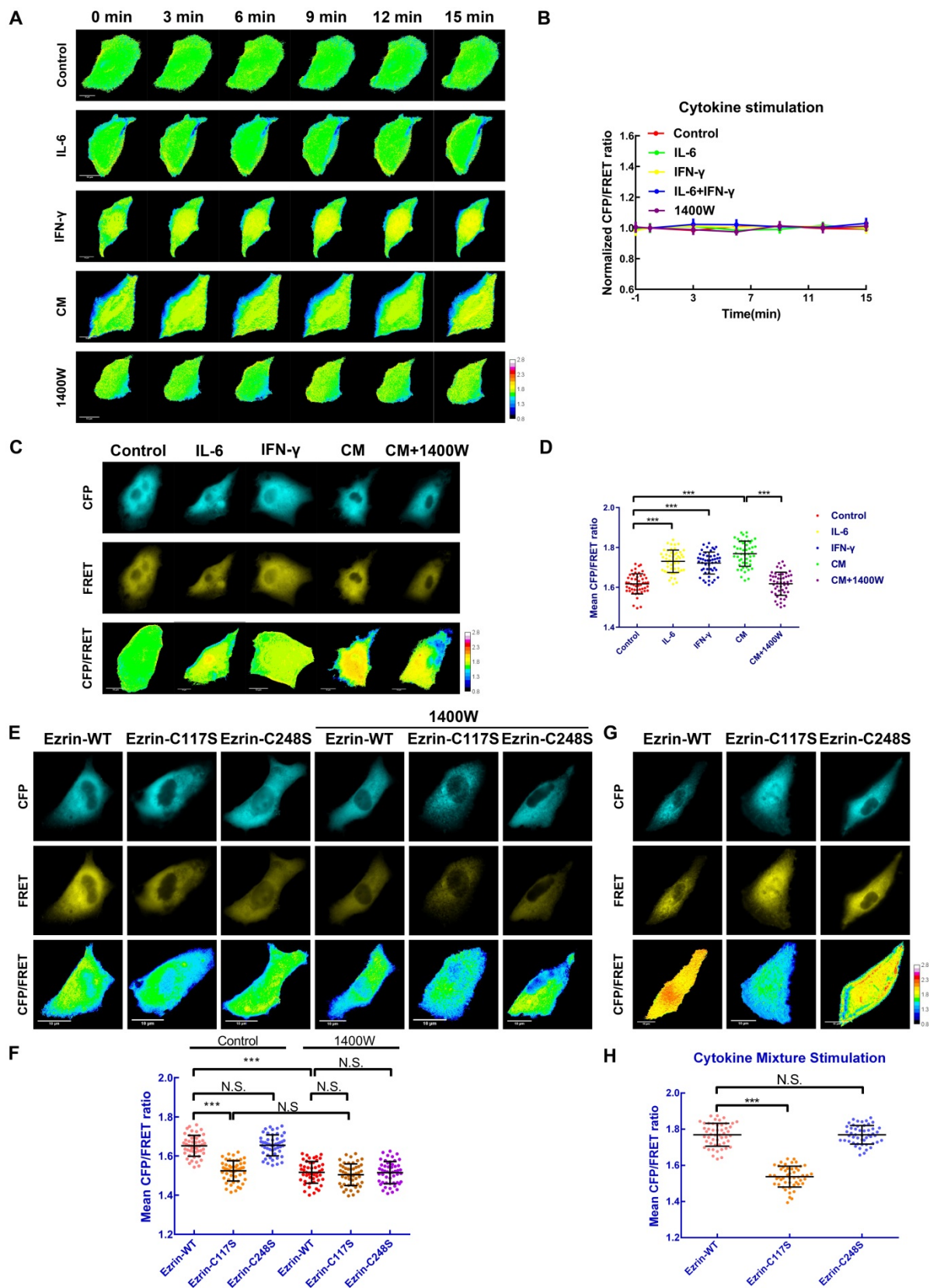


Figure 5. Ezrin-SNO on Cys¹¹⁷ results in an enhanced ezrin tension. (A) Time-lapsing imaging of ezrin-tension in cells treated with IL-6, IFN-γ, the CM, and 1400W for 15 min, respectively. **(B)** Normalized signals corresponding to ezrin tension versus time (mean ± SEM, n ≥ 5). **(C)** Representative images of FRET analysis of cells treated with IL-6, IFN-γ, the CM, and the CM+1400W for 12 h. **(D)** The means of CFP/FRET ratios are shown (mean ± SD, n = 50). **(E)** Representative images of FRET analysis of stable A549 cells expressing ezrin-M-cpstFRET, ezrin-C117S-cpstFRET, and ezrin-C248S-cpstFRET probes in both control condition and after treating with 1400W for 12 h. **(G)** Representative images of stable A549 cells expressing ezrin-M-cpstFRET, ezrin-C117S-cpstFRET, and ezrin-C248S-cpstFRET probes treated with the CM for 12 h. **(F)** and **(H)** The means of CFP/FRET ratios are shown (mean ± SD, n = 50). One-way ANOVA was used for single-factor sample comparisons. ***P < 0.001 compared with the wild-type ezrin group. Scale bar, 10 μm. The calibration bar: 0.8 to 2.8.

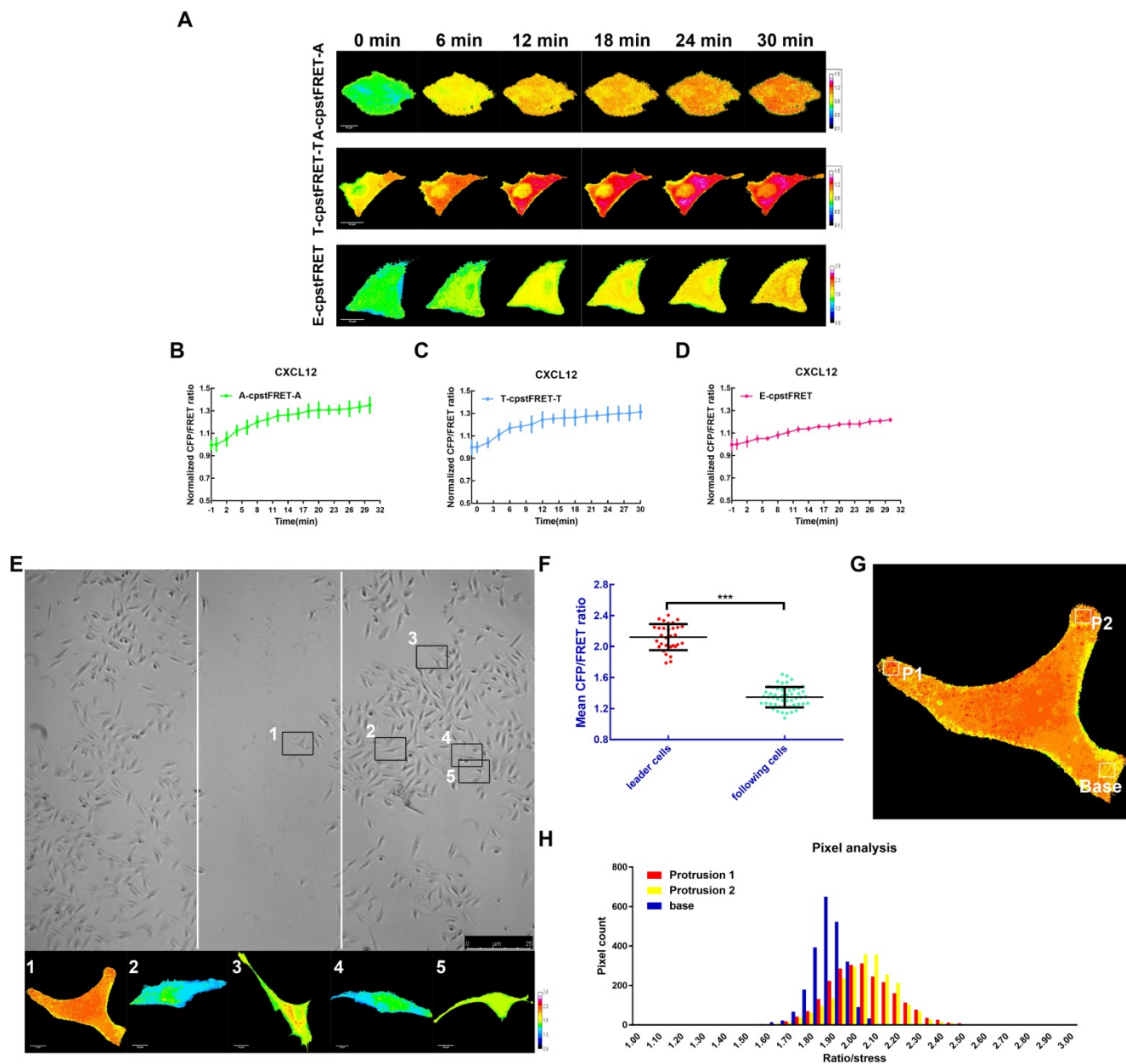


Figure 6. High ezrin tension promotes NSCLC aggressiveness. (A) 30-min time-lapsing images of FRET analysis in cells expressing A-cpstFRET-A, T-cpstFRET-T, and ezrin-M-cpstFRET probe, respectively, after CXCL12 treatment. The calibration bar: 0.1 to 1.5 for the A-cpstFRET-A and T-cpstFRET-T probes; 0.8 to 2.8 for the ezrin-M-cpstFRET probe. (B), (C), and (D) Normalized signals corresponding to MF force, MT force, and ezrin tension versus time, respectively (mean \pm SEM, $n \geq 5$). (E) Representative images of wound healing assays for cells expressing the ezrin-M-cpstFRET probe. The CFP/FRET ratio images of cells in five different positions are presented. (F) A scatter diagram showing the mean CFP/FRET ratio of both leader cells and following cells. Two-tailed Student's t-test was used for the analysis. $^{***}P < 0.001$ compared with the leader cells group. (G) and (H) Two protrusion areas (P1 and P2) and one basement area (Base) of the leader cell in (E) were selected for pixel count distribution analysis. The CFP/FRET ratio images are presented (The calibration bar: 0.8 to 2.8.) scale bar, 10 μ m.

Meanwhile, we assessed the role of ezrin tension in cancer migration using a wound healing assay combined with FRET analysis. According to the "leader cell" theory [27, 28], leader cells exhibited a higher level of ezrin tension, while that in the following cells was relatively low (Figure 6E-F). Moreover, within the leader cells, cell protrusions had relative higher ezrin tension than the basement membrane (Figure 6G-H). These data indicated that A549 cells had acquired higher ezrin tension for aggressive cell motility.

Ezrin tension coordinates with MT/MF force sensitively during NSCLC cells metastasis.

MF and MT forces are two major components of intracellular structural tension [29, 30] and the mechanical interaction between ezrin tension and MT or MF forces remains elusive. To better clarify this relationship, MF depolymerizing agent cytochalasin B (Cyto B) and MT depolymerizing agent nocodazole (Noc) were applied to disrupt cytoskeleton structure and eliminate MF or MT forces. Interestingly, CXCL12

and Cyto B co-treatment decreased ezrin tension. In CXCL12 and Noc co-treated A549 cells, ezrin tension increased more quickly than that treated with CXCL12 alone (Figure 7A-B). In addition, depolymerization of MTs and MFs simultaneously caused a sharp reduction in ezrin tension (Figure 7A-B). These findings indicate that both MT and MF forces contributed to the regulation of ezrin tension and MF forces, which may function as the major power for ezrin tension increase.

Recently, numerous researches have been done regarding to intracellular force initialized by motor proteins. Motor proteins, consisting of MT-dependent dynein and kinesin together with MF-dependent myosin [31-33], move along microtubules or microfilaments and generate forces contrary to their movement direction. These Forces generated on MT or MF structures are termed 'intracellular structural

tension' [29]. Therefore, motor protein inhibitors (Table S2) were applied to further reveal the interaction between ezrin tension and MT/MF forces. Ezrin tension increased rapidly combined with the dynein inhibitor ciliobrevin D (Cil D). By contrast, the myosin inhibitor blebbistatin (Bleb) decreased ezrin tension and the kinesin inhibitor ispinesib (Isp) maintained ezrin tension at a constant level (Figure 7C-D). Co-treatment with dynein and kinesin inhibitors disturbed the MT forces, resulting in a faster increase in ezrin tension than that in the CXCL12 group. This indicated a restraining effect of MT forces on ezrin tension. Furthermore, when all the three inhibitors were added to the aggressive model, they disrupted both the MT and MF forces, leading to a slight increase in ezrin tension. These results confirmed that MF forces contributed to the major power for ezrin tension (Figure 7C-D).

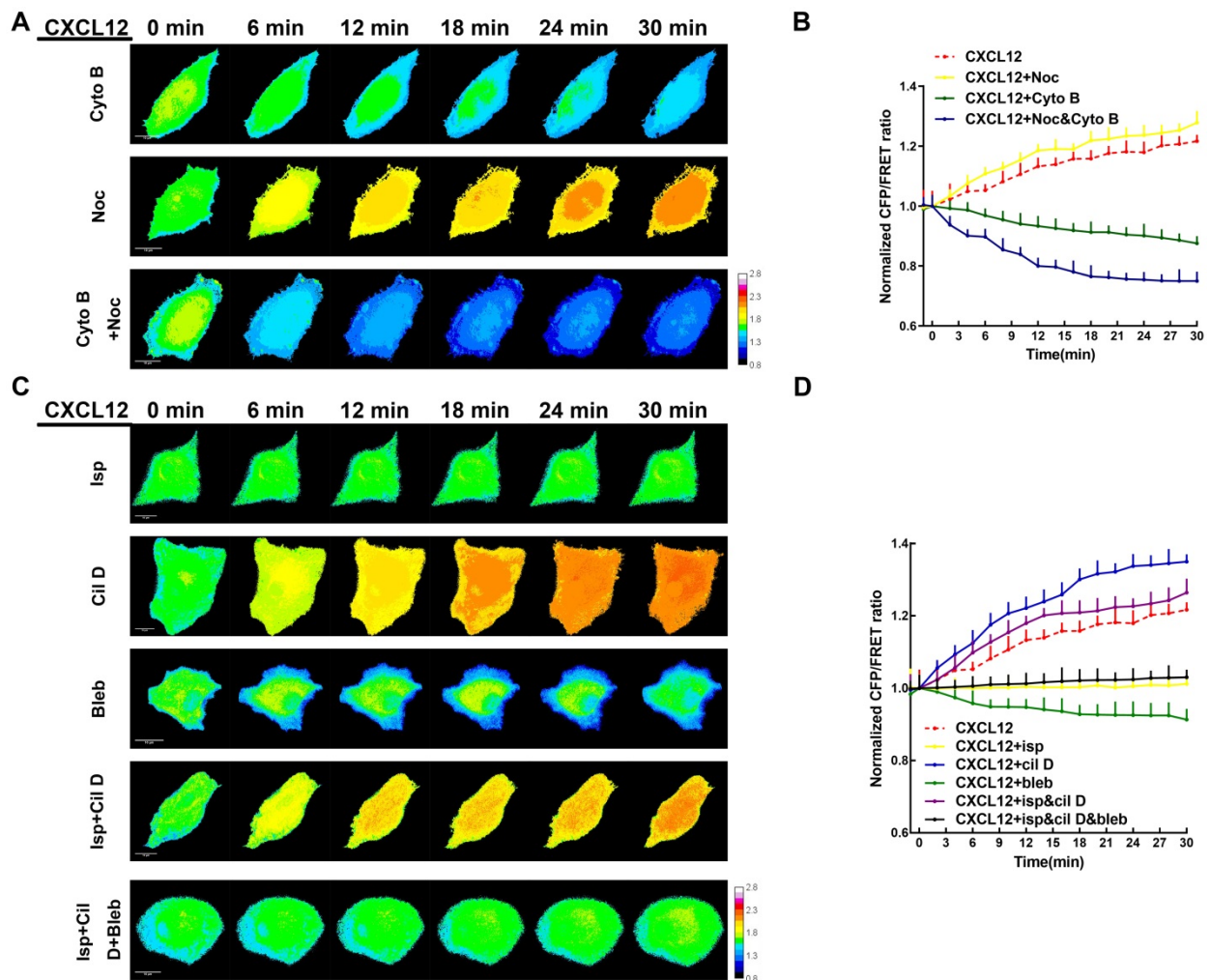


Figure 7. MT and MF forces regulate ezrin tension sensitively during NSCLC metastasis. (A) 30-min time-lapsing images of FRET analysis in cells expressing the ezrin-M-cpstFRET probe after treating with Cyto B, Noc, and Cyto B + Noc, respectively. **(C)** 30-min time-lapsing images of FRET analysis in cells expressing ezrin-M-cpstFRET probe after treating with CXCL12 in combination with Cil D, Isp, Bleb, Cil D + Isp, and Cil D + Isp + Bleb, respectively. **(B) and (D)** Normalized signals corresponding to ezrin tension versus time under different stimuli (mean± SEM, n ≥ 5). Scale bar, 10 μm. The calibration bar: 0.8 to 2.8.

Therefore, both the MT and MF forces are involved in modulating of ezrin tension during NSCLC cells motility and MF forces seem to play a dominant role in regulating ezrin tension regulation. The MT and MF forces exerted an antagonistic relationship and their resultant force resulted in increased ezrin tension which correlates with NSCLC aggressiveness.

Ezrin-SNO facilitates mechanical forces transduction.

Since ezrin-SNO promotes ezrin recruitment to the membrane, it is necessary to test whether ezrin-SNO could change the mechanical properties of

membrane-ezrin-microfilament apparatus. Therefore, we induced nitrosylation in cells expressing ezrin-WT, ezrin-C248S, and ezrin-C117S tension probes, respectively, and then challenged these cells with CXCL12. Interestingly, nitrosylated ezrin appeared more sensitive to CXCL12 treatment: The ezrin tension increased more rapidly compared with that in cells with wild-type ezrin. For ezrin-C117S, CXCL12 treatment after nitrosylation induced a slow increase in ezrin tension. By contrast, nitrosylation didn't show any changes of ezrin tension in A549 cells whether expressing mutant ezrin-C248S tension probe or wild-type ezrin (Figure 8A-B).

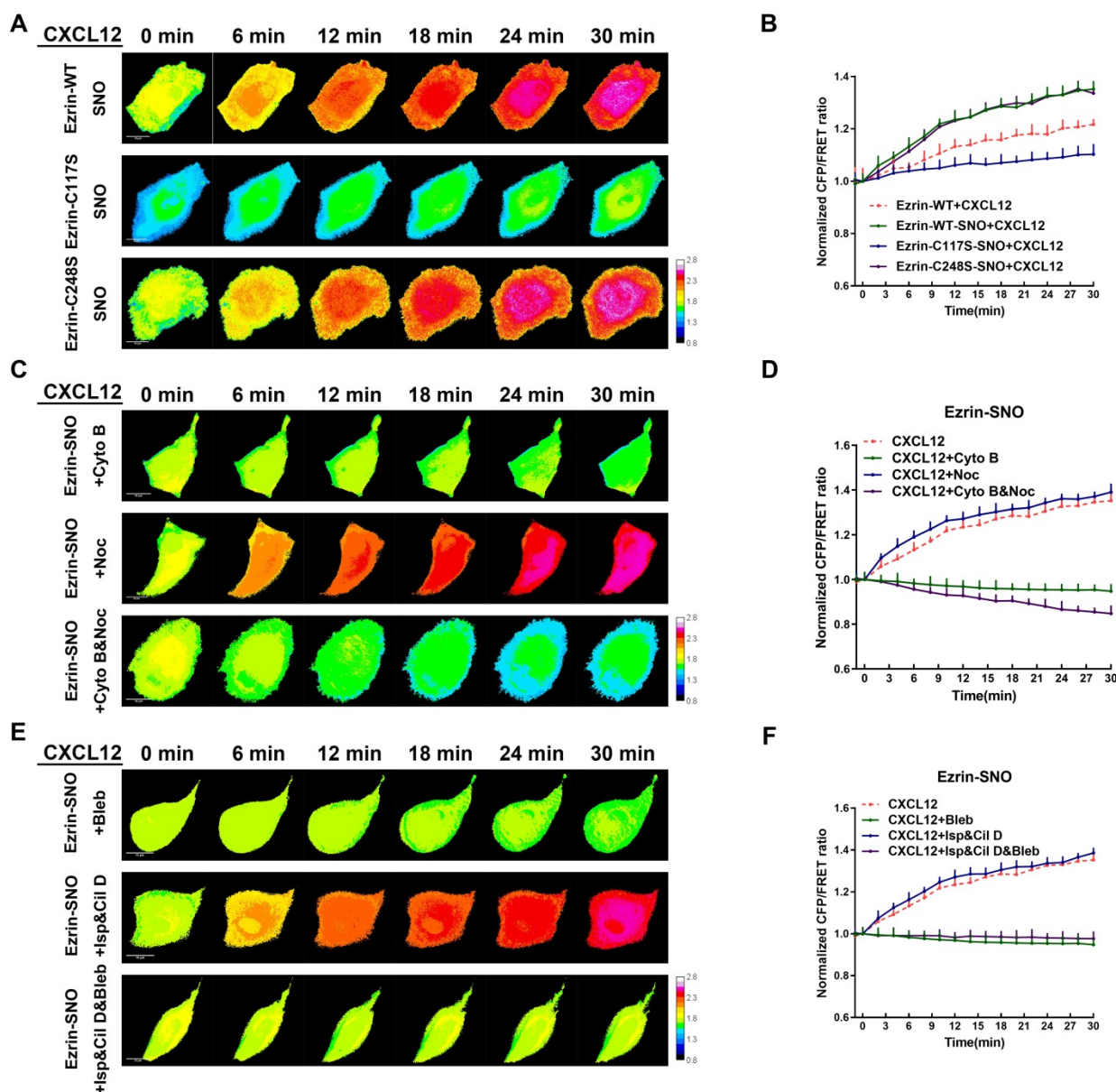


Figure 8. Ezrin-SNO contributes to more efficient mechanical transduction between the cell membrane and MF forces. (A) After the induction of nitrosylation, ezrin-M-cpstFRET, ezrin-C117S-cpstFRET and, ezrin-C248S-cpstFRET cell lines were treated with CXCL12 for 30 min. (C) After the induction of nitrosylation, ezrin-M-cpstFRET cell line was treated with Cyto B, Noc or Cyto B and Noc for 30 min, respectively. (E) After the induction of nitrosylation, ezrin-M-cpstFRET cell lines probe were treated with CXCL12 in combination with Bleb, Cil D and Isp or Cil D, Isp and Bleb together for 30 min, respectively. (B), (D), and (F) Normalized signals corresponding to ezrin tension versus time, under different stimuli (mean± SEM, n ≥ 5). Scale bar, 10 μm. The calibration bar: 0.8 to 2.8.

To test the interactions between MF/MT forces and ezrin tension after nitrosylation, we applied MT and MF depolymerizing agents again. After co-treatment with CXCL12 and Noc, nitrosylated ezrin induced increased tension similar to CXCL12 treatment alone. Moreover, decreased tension of nitrosylated ezrin was observed after treatment by CXCL12 with Cyto B. Nevertheless, treating nitrosylated cells with both Cyto B and Noc induced a slower decrease in ezrin tension compared with that in non-nitrosylated cells (Figure 8C-D).

Motor molecular inhibition experiments showed that ezrin tension increased after co-treatment with CXCL12 and two MT-related motor inhibitors at a slightly faster rate than treating with CXCL12 alone (Figure 8E-F). Moreover, the myosin inhibitor Bleb decreased ezrin tension. However, when all three kinds of motor proteins were inhibited, ezrin tension was down-regulated (Figure 8E-F).

These findings suggested a closer interaction between ezrin tension and MF forces after nitrosylation, inversely, MT force exhibited less impact on ezrin tension modulation. As a result, ezrin tension augmented during CXCL12 stimulation reached a higher level, possibly representing a higher aggressiveness.

Discussion

Protein S-nitrosylation is involved in various cancer progression [34-37]. In lung cancer, the complex inflammatory microenvironment results in abundant iNOS expression, [5, 6, 38] facilitating nitrosylation of various proteins. In the present study, we showed that ezrin-SNO was positively related to aggressiveness of NSCLC cells and poor clinical outcome of patients. The experimental evidence allowed us to hypothesize that S-nitrosylation-related up-regulation of ezrin function is correlated with the aggressive behavior of NSCLC cells.

In normal lung tissue and A549 cells, low levels of ezrin-SNO were detected (Figure 1C-D, Figure 2C-D, Figure S1A-B), suggesting a physiological role of ezrin-SNO in cell biology. With the gradual recognition of protein nitrosylation in pulmonary physiology, aberrant level of nitrosylated proteins in lung carcinoma have received more attention [38]. The nitrosylation of ezrin is target-selective, and our experiments revealed that Cys¹¹⁷ of ezrin was the only active site accepting a NO group. Ezrin Cys¹¹⁷ seems to be a potential target to regulate NSCLC cells invasion and metastasis.

As a linker between the membrane and microfilaments, ezrin is involved in intracellular mechanical activities that are important in cancer motility [13]. The development of a FRET-based ezrin

tension probe made it possible to collect real-time data and precisely assess its mechanical activity in live cells. During NSCLC cells invasion and metastasis, ezrin tension was relatively high (Figure 6). Ezrin is considered as a marker for malignancy and poor prognosis, and as a major component of aggression-related structures, such as filopodia, lamellipodia, and invadopodia. Therefore, we speculated that high ezrin tension would correlate with malignant motilities and the formation of aggressive structures in NSCLC cells.

Ezrin, as a linker protein, is unable to generate forces. Therefore, it is necessary to investigate the derivation of ezrin tension. Cytoskeleton depolymerization and motor inhibition experiments suggested that MF, but not MT, forces exert the major power for increased ezrin tension (Figure 7). The close relationship between MFs and ezrin structure make it easy to understand that MF forces are the most important regulator of ezrin tension. However, unexpectedly, MT forces also participated in the regulation of ezrin tension. Indeed, the mutual interaction between MTs and ERM proteins has been reported [39]. The connection of MFs and MTs via intermediate filaments and other linker proteins maintains cytoskeletal integrity for mechanical transduction [40]. Therefore, it is possible that MT forces have a direct or indirect impact on ezrin tension. Notably, MF forces exhibited an antagonistic reciprocity with MT forces in modulating ezrin tension (Figure 7). Meanwhile, ezrin-SNO tended to translocate to the cell membrane (Figure 3E), and the mechanical interaction between ezrin and MFs seemed to be more intimate (Figure 8C-F). Furthermore, nitrosylated ezrin exhibited a more sensitive response to CXCL12 treatment, with a faster and larger tension increase. These data suggested that NSCLC cells acquired better plasticity in response to chemokine-associated mechanical effect after ezrin-SNO. Recent studies using atomic force microscope (AFM) revealed that many kinds of cancer cells such as breast [41], lung [42], liver[43] and ovarian[44] cancer usually appear with an decreased Young's modulus, which represents softness of cells during transformation from the non-malignant stage to the aggressive stage or from normal cells to pre-malignant and malignant cells. MFs and MTs act as master regulators of cell shape [45, 46] and MTs function to withstand compressing forces from the cell cortex [47], which are generated by actomyosin networks [48]. Therefore, considering the nucleus as the center of a cell, MTs intend to generate an outward force, while the actin cortex generates an inward force. The joint effect of outward MT and inward MF forces controls the cell shape and plasticity. In cancer

cells with a malignant phenotype, up-regulated ezrin-SNO could promote membrane-MF interactions as anchors, such that MF forces could exert more efficient contractility on the membrane. As a result, inward MF forces are capable to compress outward MT forces, finally reaching a new balance, in which the cell membrane becomes more flexible and easier to invade and metastasize. Collectively, this pathological alteration correlating with ezrin-SNO might facilitate cellular mechanical transduction and promote NSCLC cells invasion and metastasis.

Cancer cell invasion and migration underlie metastatic dissemination, which is one of the major problems in cancer. In the present study, ezrin demonstrated a high relevance to cancer motility from the perspective of subcellular structural tension. According to the data obtained from traction force microscopy, during collective migration, there is a force gradient from the leading edge to the rear of the cell collective which was termed the 'tug-of-war model' and leader cells undertakes a higher traction force [49]. Similarly, our study showed that leader cells exhibited a higher ezrin tension compared with that in following cells, and acted as a locomotive power for multicellular migration (Figure 6E-F). Besides, ezrin tension in cell protrusions toward the migration direction reached a relatively high level, while ezrin tension in the basement membrane was relative low (Figure 6G-H). Ezrin promotes membrane blebbing [50] which are precursors of mature membrane structures such as filopodia and lamellipodia [51]. Moreover, enhanced MF forces are distributed along the free edges of leader cells and inhibition of MF forces can suppress leading cell formation [52]. Collectively, we speculated that leader cells are also characterized by enhanced subcellular tension, and the formation of membrane protrusions may be highly related to enhanced ezrin tension, which is mainly regulated by MF forces. Cancer cells, especially leader cells, need to generate high levels of intracellular force in leading positions to overcome resistance outside the cells.

With regard to individual cell migration, the present study suggested a positive role of subcellular mechanics, especially ezrin tension, in promoting cancer motility (Figure 6A-D). Actually, both MT and MF forces are involved in different phases of cell migration [46, 53]. However, according to our results, MF forces act as the major modulator of ezrin tension, which is relevant to cancer motility. Enhanced MF forces have been reported to participate in membrane protrusion formation [54], which results in individual cell migration. Recent studies concerning individual cell migration have revealed a complex process which is described as 'mesenchymal-amoeboid plasticity'

[55]. We attempted to extend our findings and analyze the function of MF forces together with ezrin tension in membrane protrusion formation. The first step is the formation of membrane blebs which depends on either local membrane detachment or cortex rupture [56]. As a result, a softening of the local cortical periphery occurs. Thereafter, activated Rho-ROCK and Cdc42-MRCK signaling enhance myosin II-based contractile forces [53]. This increased trend of MF forces was detected (Figure 6A-B). Meanwhile pulling by the enhanced MF force, ezrin tension increased gradually (Figure 6A, D). The increased MF forces could generate a local high pressure area, which act as the driving force to squeeze the softened cell surface into a bleb that bulges out of cell body. Subsequently, local pressure continues to drive bleb expansion and the flow of cytosol into the bleb increases its volume [54]. To sustain the shape change, the conserved and rigid MT structures [45] begin to exert tractive forces, consequently generating antagonistic MT forces to restrain MF forces, as well as ezrin tension. However, because of the different magnitude of the forces, the MF forces overwhelm the MT forces, leading to a continuously extending cell protrusion, as well as a relatively high ezrin tension (Figure 6A). With the rapid assembly of actomyosin networks [54], mature structures begin to take shape.

Conclusions

This study provides evidence that nitrosylation of ezrin may promote NSCLC aggressiveness as a mechanical mediator. The interaction between membrane proteins and ezrin tension, as well as the mechanism of membrane-to-cytoskeleton mechanical signaling in cancer motility, warrants further examination. Besides, drug development strategies targeting ezrin-SNO and its mechanical transduction may represent potential therapeutic approaches to inhibit NSCLC progression and may open new perspectives for the treatment of cancer.

Abbreviations

NSCLC: non-small cell lung cancer; SNO: S-nitrosylation; FRET: Förster resonance energy transfer; NO: nitric oxide; NOS: NO synthase; iNOS: inducible NOS; MF: microfilament; MT: microtubule; TNF- α : tumor necrosis factor alpha; IL: interleukin; IFN- γ : interferon- γ ; ERM: ezrin-radixin-moesin; ATCC: American Type Culture Collective; STR: short tandem repeat; CXCL12: C-X-C motif chemokine 12; L-NMMA: L-NG-monomethyl arginine citrate; FITC: isothiocyanate; TRITC: tetramethylrhodamine; DAPI: 4, 6-diamidino-2-phenylindole; siRNA: Small interfering RNA; cpstFRET: circularly permuted

stretch sensitive FRET module; DV-2: dual-view-2; EX: excitation wavelength; EM: emission wavelength; ANOVA: one-way analysis of variance; CM: cytokine mixture; FRET-AB: acceptor bleaching FRET test; FRAP: fluorescence recovery after photobleaching; ROI: region of interest; Cyto B: cytochalasin B; Noc: nocodazole; Cil D: ciliobrevin D; Bleb: (-)-blebbistatin; Isp: ispinesib; AFM: atomic force microscope.

Supplementary Material

Supplementary figures and tables.

<http://www.thno.org/v09p2555s1.pdf>

Acknowledgements

This work was supported by grants from the National Natural Science Foundation of China (81573409) and Natural Science Foundation of Jiangsu Province (BK20161574) and A Project Funded by the Priority Academic Program Development of Jiangsu Higher Education Institutions (Integration of Raditional Chinese and Western Medicine) and Postgraduate Research & Practice Innovation Program of Jiangsu Province (KYCX18_1563).

Contributions

Jun Guo and Bin Ren conceived the experiment. Xiaolong Zhang, Yifan Wang, Ying Song, Yunfeng Hu and Jingwen Zhou performed the experiments. Xiaolong Zhang, Yichen Guo, Yifan Wang, Lixia Sun analyzed and interpreted the data. Xiaolong Zhang, Guangming Li, Qinli Ruan and Linlin Chen wrote the manuscript. All authors read and approved the final manuscript.

Competing Interests

The authors have declared that no competing interest exists.

References

1. Siegel RL, Miller KD, Jemal A. Cancer statistics, 2018. *CA Cancer J Clin*. 2018; 68: 7-30.
2. Steeg PS. Tumor metastasis: mechanistic insights and clinical challenges. *Nat Med*. 2006; 12: 895-904.
3. Doulias PT, Greene JL, Greco TM, Tenopoulou M, Seeholzer SH, Dunbrack RL, et al. Structural profiling of endogenous S-nitrosocysteine residues reveals unique features that accommodate diverse mechanisms for protein S-nitrosylation. *Proc Natl Acad Sci U S A*. 2010; 107: 16958-63.
4. Salim T, Sershen CL, May EE. Investigating the Role of TNF-alpha and IFN-gamma Activation on the Dynamics of iNOS Gene Expression in LPS Stimulated Macrophages. *PLoS One*. 2016; 11: e0153289.
5. Elinav E, Nowarski R, Thaiss CA, Hu B, Jin C, Flavell RA. Inflammation-induced cancer: crosstalk between tumours, immune cells and microorganisms. *Nat Rev Cancer*. 2013; 13: 759-71.
6. Guo FH, Uetani K, Haque SJ, Williams BR, Dweik RA, Thunnissen FB, et al. Interferon gamma and interleukin 4 stimulate prolonged expression of inducible nitric oxide synthase in human airway epithelium through synthesis of soluble mediators. *J Clin Invest*. 1997; 100: 829-38.
7. Chi DS, Qui M, Krishnaswamy G, Li C, Stone W. Regulation of nitric oxide production from macrophages by lipopolysaccharide and catecholamines. *Nitric Oxide*. 2003; 8: 127-32.
8. Wang Z. Protein S-nitrosylation and cancer. *Cancer Lett*. 2012; 320: 123-9.
9. Moldogazieva NT, Lutsenko SV, Terentiev AA. Reactive Oxygen and Nitrogen Species-Induced Protein Modifications: Implication in Carcinogenesis and Anticancer Therapy. *Cancer Res*. 2018; 78: 6040-7.

10. Fehon RG, McClatchey AI, Bretscher A. Organizing the cell cortex: the role of ERM proteins. *Nat Rev Mol Cell Biol*. 2010; 11: 276-87.
11. Li Q, Gao H, Xu H, Wang X, Pan Y, Hao F, et al. Expression of ezrin correlates with malignant phenotype of lung cancer, and in vitro knockdown of ezrin reverses the aggressive biological behavior of lung cancer cells. *Tumour Biol*. 2012; 33: 1493-504.
12. Lallemand D, Arpin M. Moesin/ezrin: a specific role in cell metastasis? *Pigment Cell Melanoma Res*. 2010; 23: 6-7.
13. Kumar S, Weaver VM. Mechanics, malignancy, and metastasis: the force journey of a tumor cell. *Cancer Metastasis Rev*. 2009; 28: 113-27.
14. Bretscher A, Edwards K, Fehon RG. ERM proteins and merlin: integrators at the cell cortex. *Nat Rev Mol Cell Biol*. 2002; 3: 586-99.
15. Wang Y, Zhang X, Tian J, Shan J, Hu Y, Zhai Y, et al. Talin promotes integrin activation accompanied by generation of tension in talin and an increase in osmotic pressure in neurite outgrowth. *FASEB J*. 2019; 10.1096/fj.201801949RR.
16. Guo J, Wang Y, Sachs F, Meng F. Actin stress in cell reprogramming. *Proc Natl Acad Sci U S A*. 2014; 111: E5252-61.
17. Gyorffy B, Surowiak P, Budczies J, Lanczky A. Online survival analysis software to assess the prognostic value of biomarkers using transcriptomic data in non-small-cell lung cancer. *PLoS One*. 2013; 8: e82241.
18. Caetano MS, Zhang H, Cumpian AM, Gong L, Unver N, Ostrin EJ, et al. IL6 Blockade Reprograms the Lung Tumor Microenvironment to Limit the Development and Progression of K-ras-Mutant Lung Cancer. *Cancer Res*. 2016; 76: 3189-99.
19. Clucas J, Valderrama F. ERM proteins in cancer progression. *J Cell Sci*. 2014; 127: 267-75.
20. Meng F, Sachs F. Orientation-based FRET sensor for real-time imaging of cellular forces. *J Cell Sci*. 2012; 125: 743-50.
21. Chen T, Guo Y, Shan J, Zhang J, Shen X, Guo J, et al. Vector Analysis of Cytoskeletal Structural Tension and the Mechanisms that Underpin Spectrin-Related Forces in Pyroptosis. *Antioxid Redox Signal*. 2018; 10.1089/ars.2017.7366
22. Wakayama T, Nakata H, Kurobo M, Sai Y, Iseki S. Expression, localization, and binding activity of the ezrin/radixin/moesin proteins in the mouse testis. *J Histochem Cytochem*. 2009; 57: 351-62.
23. Murphy DA, Courtneidge SA. The 'ins' and 'outs' of podosomes and invadopodia: characteristics, formation and function. *Nat Rev Mol Cell Biol*. 2011; 12: 413-26.
24. Collin O, Na S, Chowdhury F, Hong M, Shin ME, Wang F, et al. Self-organized podosomes are dynamic mechanosensors. *Curr Biol*. 2008; 18: 1288-94.
25. Mantovani A. Chemokines in neoplastic progression. *Semin Cancer Biol*. 2004; 14: 147-8.
26. Phillips RJ, Burdick MD, Lutz M, Belperio JA, Keane MP, Strieter RM. The stromal derived factor-1/CXCL12-CXC chemokine receptor 4 biological axis in non-small cell lung cancer metastases. *Am J Respir Crit Care Med*. 2003; 167: 1676-86.
27. Poujade M, Grasland-Mongrain E, Hertzog A, Jouanneau J, Chavrier P, Ladoux B, et al. Collective migration of an epithelial monolayer in response to a model wound. *Proc Natl Acad Sci U S A*. 2007; 104: 15988-93.
28. Khalil AA, Friedl P. Determinants of leader cells in collective cell migration. *Integr Biol (Camb)*. 2010; 2: 568-74.
29. Guo YC, Wang YX, Ge YP, Yu LJ, Guo J. Analysis of subcellular structural tension in axonal growth of neurons. *Rev Neurosci*. 2018; 29: 125-37.
30. Zhang J, Wang Y, Zheng Z, Sun X, Chen T, Li C, et al. Intracellular ion and protein nanoparticle-induced osmotic pressure modify astrocyte swelling and brain edema in response to glutamate stimuli. *Redox Biol*. 2019; 21: 101-12.
31. Firestone AJ, Weinger JS, Maldonado M, Barlan K, Langston LD, O'Donnell M, et al. Small-molecule inhibitors of the AAA+ ATPase motor cytoplasmic dynein. *Nature*. 2012; 484: 125-9.
32. Lad L, Luo L, Carson JD, Wood KW, Hartman JJ, Copeland RA, et al. Mechanism of inhibition of human KSP by ispinesib. *Biochemistry*. 2008; 47: 3576-85.
33. Medeiros NA, Burnette DT, Forscher P. Myosin II functions in actin-bundle turnover in neuronal growth cones. *Nat Cell Biol*. 2006; 8: 215-26.
34. Romagny S, Bouaouiche S, Lucchi G, Ducoroy P, Bertoldo JB, Terenzi H, et al. S-Nitrosylation of cIAP1 Switches Cancer Cell Fate from TNFalpha/TNFR1-Mediated Cell Survival to Cell Death. *Cancer Res*. 2018; 78: 1948-57.
35. Kim J, Choi S, Saxena N, Singh AK, Singh I, Won JS. Regulation of STAT3 and NF-kappaB activations by S-nitrosylation in multiple myeloma. *Free Radic Biol Med*. 2017; 106: 245-53.
36. Burke AJ, Garrido P, Johnson C, Sullivan FJ, Glynn SA. Inflammation and Nitrosative Stress Effects in Ovarian and Prostate Pathology and Carcinogenesis. *Antioxid Redox Signal*. 2017; 26: 1078-90.
37. Shen X, Burguillos MA, Osman AM, Frijhoff J, Carrillo-Jimenez A, Kanatani S, et al. Glioma-induced inhibition of caspase-3 in microglia promotes a tumor-supportive phenotype. *Nat Immunol*. 2016; 17: 1282-90.
38. Guo C, Atochina-Vasserman E, Abramova H, George B, Manoj V, Scott P, et al. Role of NOS2 in pulmonary injury and repair in response to bleomycin. *Free Radic Biol Med*. 2016; 91: 293-301.
39. Solinet S, Mahmud K, Stewman SF, Ben El Kadhi K, Decelle B, Talje L, et al. The actin-binding ERM protein Moesin binds to and stabilizes microtubules at the cell cortex. *J Cell Biol*. 2013; 202: 251-60.

40. Fletcher DA, Mullins RD. Cell mechanics and the cytoskeleton. *Nature*. 2010; 463: 485-92.
41. Schierbaum N, Rheinlaender J, Schaffer TE. Viscoelastic properties of normal and cancerous human breast cells are affected differently by contact to adjacent cells. *Acta Biomater*. 2017; 55: 239-48.
42. Plodinec M, Loparic M, Monnier CA, Obermann EC, Zanetti-Dallenbach R, Oertle P, et al. The nanomechanical signature of breast cancer. *Nat Nanotechnol*. 2012; 7: 757-65.
43. Tian M, Li Y, Liu W, Jin L, Jiang X, Wang X, et al. The nanomechanical signature of liver cancer tissues and its molecular origin. *Nanoscale*. 2015; 7: 12998-3010.
44. Babahosseini H, Ketene AN, Schmelz EM, Roberts PC, Agah M. Biomechanical profile of cancer stem-like/tumor-initiating cells derived from a progressive ovarian cancer model. *Nanomedicine*. 2014; 10: 1013-9.
45. Blanchoin L, Boujemaa-Paterski R, Sykes C, Plastino J. Actin dynamics, architecture, and mechanics in cell motility. *Physiol Rev*. 2014; 94: 235-63.
46. Bouchet BP, Akhmanova A. Microtubules in 3D cell motility. *J Cell Sci*. 2017; 130: 39-50.
47. Ingber DE. Tensegrity I. Cell structure and hierarchical systems biology. *J Cell Sci*. 2003; 116: 1157-73.
48. Clark AG, Wartlick O, Salbreux G, Paluch EK. Stresses at the cell surface during animal cell morphogenesis. *Curr Biol*. 2014; 24: R484-94.
49. Riahi R, Sun J, Wang S, Long M, Zhang DD, Wong PK. Notch1-Dll4 signalling and mechanical force regulate leader cell formation during collective cell migration. *Nat Commun*. 2015; 6: 6556.
50. Hinojosa LS, Holst M, Baarlink C, Grosse R. MRTF transcription and Ezrin-dependent plasma membrane blebbing are required for entotic invasion. *J Cell Biol*. 2017; 216: 3087-95.
51. Bergert M, Chandradoss SD, Desai RA, Paluch E. Cell mechanics control rapid transitions between blebs and lamellipodia during migration. *Proc Natl Acad Sci U S A*. 2012; 109: 14434-9.
52. Reffay M, Parrini MC, Cochet-Escartin O, Ladoux B, Buguin A, Coscoy S, et al. Interplay of RhoA and mechanical forces in collective cell migration driven by leader cells. *Nat Cell Biol*. 2014; 16: 217-23.
53. Charras GT, Yarrow JC, Horton MA, Mahadevan L, Mitchison TJ. Non-equilibration of hydrostatic pressure in blebbing cells. *Nature*. 2005; 435: 365-9.
54. Charras G, Paluch E. Blebs lead the way: how to migrate without lamellipodia. *Nat Rev Mol Cell Biol*. 2008; 9: 730-6.
55. Wolf K, Mazo I, Leung H, Engelke K, von Andrian UH, Deryugina EI, et al. Compensation mechanism in tumor cell migration: mesenchymal-amoeboid transition after blocking of pericellular proteolysis. *J Cell Biol*. 2003; 160: 267-77.
56. Boulbitch A, Simson R, Simson DA, Merkel R, Hackl W, Barmann M, et al. Shape instability of a biomembrane driven by a local softening of the underlying actin cortex. *Phys Rev E Stat Phys Plasmas Fluids Relat Interdiscip Topics*. 2000; 62: 3974-85.